Simulation of Electro-Discharge Dynamic Disintegration of Concrete Members Using a 3D Fluid-Structure Interaction Elasto-Plastic Fracture Model

3 次元流体－構造連成弾塑性破壊モデルによる コンクリート部材の放電衝撃破砕シミュレーション

ADDISU BONGER*[1], RANKOTH CHAMILA*[1], HIROO SHINOZAKI*[1]
アディス　ボンガー，ランコス　チャミラ，篠崎　裕生

This study attempts to numerically reproduce the Electric Discharge Impulse Crushing System (EDICS) technology which utilizes self-reactive liquid deflagration for controlled dismantling of concrete members. A three-dimensional dynamic nonlinear finite element analysis was performed using an elasto-plastic fracturing model integrated with poro-mechanical approach, that captures blast-induced concrete fracture by accounting for gas kinetics within crack networks. The analysis confirmed that pressurized gas widened and propagated concrete cracks, and the primary fracture surface formed at a location similar to that observed in the experiments. In addition, increasing the number of studs enhanced the confinement effect on the concrete, leading to greater gas pressure buildup and more extensive damage.

Keywords: Deflagration, Bridge Deck Removal, Finite Element Method, Elasto-Plastic Fracture Model

本報は，ニトロメタンの爆燃を利用したコンクリート部材の放電衝撃破砕技術（EDICS）について数値解析による再現を試みたものである。解析には，コンクリート空隙内圧力の増大による亀裂の進展と損傷とを再現できる新しい弾塑性破壊モデルを組み込んだ 3 次元動的非線形有限要素解析を用いた。解析の結果，加圧されたガスがひび割れを拡幅・進展させること，主たる破壊面が実験と同様な位置に形成されること，また，スタッド数の増加によりコンクリートの拘束効果が高まり，ガス圧の上昇が著しくなるとともに損傷がより広範囲に及ぶことが確認された。

キーワード：放電衝撃破砕，床版解体，有限要素法，弾塑性破壊モデル

1. Introduction

As aging infrastructure increasingly requires partial or complete demolition for reconstruction, urban redevelopment, and emergency operations, there is a growing demand for safe, efficient, and controllable demolition methods. Conventional explosive blasting enables rapid demolition but poses significant risks in densely populated areas due to uncontrolled energy release and potential overcharging[1)]. To overcome these limitations, the Electric Discharge Impulse Crushing System (EDICS), which utilizes the controlled deflagration of self-reactive liquid triggered by a high-voltage electrical discharge, has been developed as a practical and precise demolition technique[2)]. Compared with conventional explosives, deflagration generates lower pressures and more moderate structural damage, offering enhanced controllability[3)].

This study targets the removal of existing concrete deck slabs during the rehabilitation of steel-concrete composite girder bridges, with the objective of preserving the steel girders for subsequent reuse. In this context, the present study investigates the fracture mechanisms of steel-concrete composite structures subjected to deflagration using numerical

*[1] Research & Development Institute, Technology Development Promotion Department

simulation. Advanced three-dimensional dynamic nonlinear finite element analyses are conducted to characterize the structural response and evaluate the effectiveness of controlled concrete deck demolition while ensuring the integrity of the steel girders. The numerical simulation was verified against the experimental observations of crack propagation. Following this verification, the model was employed to investigate the effects of gas pressure, yielding state of the steel girder, and the influence of explosion speed on the structural response. These aspects could not be verified experimentally because quantitative measurements were not available in the experimental program.

2. Multiscale Poro-mechanical Modeling

In this study, internal blast demolition was performed on a steel-concrete composite structure to remove the concrete deck slab while preventing the steel girder from yielding. Therefore, evaluating the post-demolition stress levels in the steel components was essential to verify that the steel girder remained below its yield limit. Elastic wave simulation can predict the initial stress-wave propagation but cannot account for nonlinear concrete fracture, stiffness degradation, and gas-driven crack propagation, which governs the load transfer between damaged concrete and steel. In this study, elastic wave simulation was not considered because the stress response of the steel components is strongly affected by the progressive interaction between fractured concrete, pressurized gases, and steel members. Instead, a highly nonlinear poro-mechanical FEM approach was employed to capture these mechanisms and reliably assess whether the steel girder remains below the yield limit after the explosion.

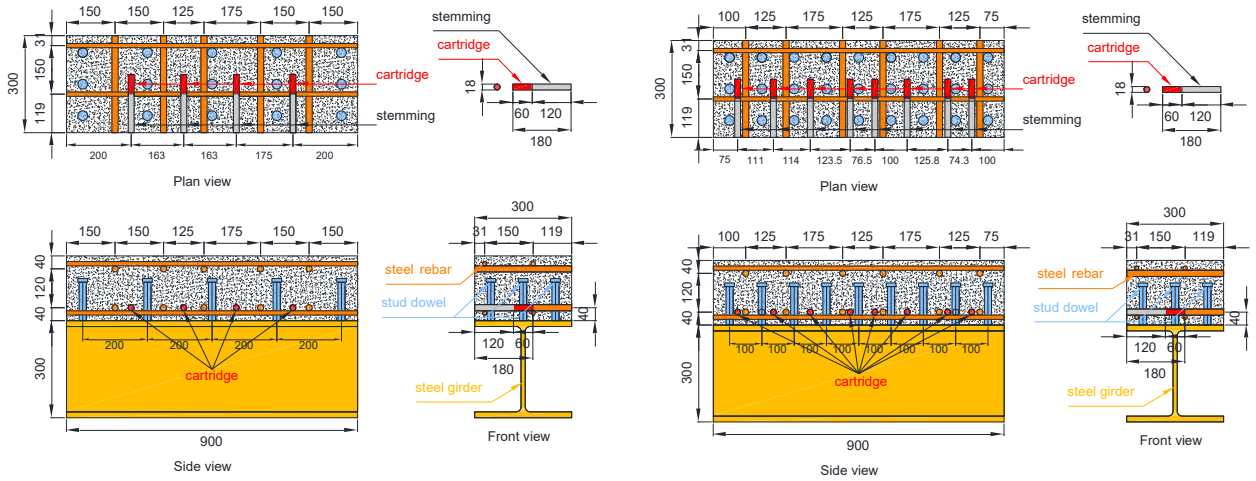
The analysis method in this study is based on a novel poro-mechanical approach to analyze blast induced fracture in concrete considering gaseous kinetics[4]. In this method, the Biot equations[5),6)], which are the fundamental equations describing the interaction between the solid skeleton and pore fluid in porous materials, are extended to compressible fluid media with nonconstant density that varies according to pore pressure. The analysis method targets three specific aspects: (1) concrete as a nonlinear porous material with initial porosity; (2) multidirectional crack interaction across three dimensions; and (3) accounting for phase changes between liquid and gas. The approach is integrated within a multiscale computational framework that couples and analyzes physical phenomena across multiple scales, from material behavior to structural response[7)] and utilizes an elasto-plastic fracturing model to solid concrete that considers strain-rate effects, and 3D confinement. Stresses are calculated by directly integrating the strain history within each finite element, while post-cracking behavior is represented through a multi-directional, non-orthogonal post-cracking model incorporating compression, tension, shear transfer, and reinforcement–concrete bond mechanisms. Furthermore, severe damage phenomena such as concrete graveling under high shear and compressive stresses are included[8)], enabling a comprehensive simulation of fracture processes in concrete structures subjected to explosive loading.

3. Referenced Specimen and Simulation Model

The experimental findings obtained on two specimens presented in previous research[9)] were utilized as a reference of verification and validation of the simulation. **Fig. 1** illustrates the plane, side and front views of the two steel-concrete composite structures. The structure is composed of a reinforced concrete slab on top of a steel girder and stud dowels having a diameter of 22 mm and a height of 130 mm. In the slab of dimensions 900 mm × 300 mm × 200 mm, blast holes that can hold the cartridges (energy sources) containing the self-reactive liquid are drilled and covered by stemming material. The bars indicated in orange are steel rebars, and the blue and red sections in the figure are the stud dowels and cartridges producing electric discharge deflagration. The distinct dissimilarity between the two types of specimens, specimen A **(Fig. 1(a))** and specimen B (**Fig. 1(b)**), is the horizontal spatial distance (ΔL) between each stud dowel in the direction of the axis of the specimen. The distance ΔL is 200 mm for the specimen A and 100 mm for the specimen B. Accordingly, the cartridges set in the specimen B are double in number.

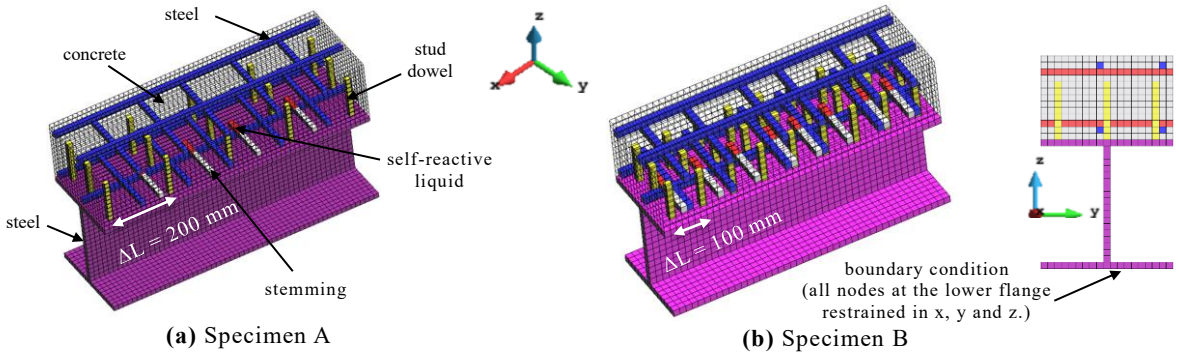
Finite element model was discretized using hexahedral finite elements (1.4 cm mesh size) as shown in **Fig. 2**[10)]. Material properties were assigned to each element representing concrete and stemming as lined up in **Table 1**. The

tension softening model for plain concrete is taken into account by c parameter (Equation (1)) that is determined from fracture energy of concrete and the reference length of the finite element[11]. Steel rebars, stud dowels and steel girders were defined by a perfectly plastic bilinear material mode with Young's modulus E = 210 GPa and yield strength f_{yt} = 400 MPa. The upper steel plate (flange) of the girder is perfectly bonded to the concrete slab. The energy release of self-reactive liquid was defined by the time of initiation of deflagration t_{start} and t_{peak} when pressure reaches its maximum p_{peak} and the density ρ as shown in **Table 2**.



(a) Specimen A **(b)** Specimen B

Fig. 1. Dimensions of two referenced specimens [unit: mm][9]



(a) Specimen A **(b)** Specimen B

Fig. 2. 3D finite element

Table 1. Material properties[10]

	Unit	Concrete	Stemming
Young's modulus	GPa	34.2	0.08
Compressive strength	MPa	31	1
Tensile strength	MPa	2.6	0.1
Density	kg/m^3	2300	1800
Permeability	cm/s	10^{-7}	10^{-1}
Porosity	(-)	0.02	0.4
Tension softening factor	(-)	1.0	2.0

Table 2. Material properties of self-reactive liquid[10]

	t_{start} (μs)	t_{peak} (μs)	p_{peak} (GPa)	ρ (g/cm^3)
Specific figures of self-reactive liquid	0	55	1.1	1.14

$$\int \sigma_t d\varepsilon_t = \int f_t \left(\frac{\varepsilon_{tu}}{\varepsilon_t}\right)^c d\varepsilon_t = \frac{G_f}{l_r} \quad (1)$$

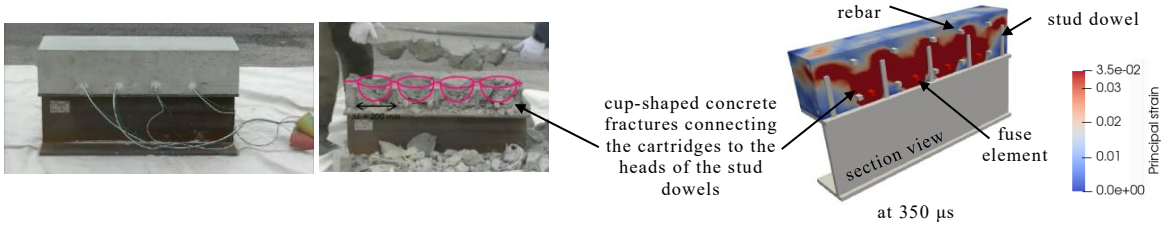
where σ_t is tensile stress, f_t is uniaxial tensile strength, ε_{tu} is cracking strain, ε_t is average tensile strain, G_f is fracture energy and l_r is finite element length.

4. Numerical Simulation

The simulation was conducted to verify the final cracking patterns and concrete damage against the experimental observations. In addition, it was used to investigate the migration of pressurized gas and its effect on crack propagation and to evaluate the stress distribution in the steel girder for assessing potential yielding, for which experimental measurements were unavailable.

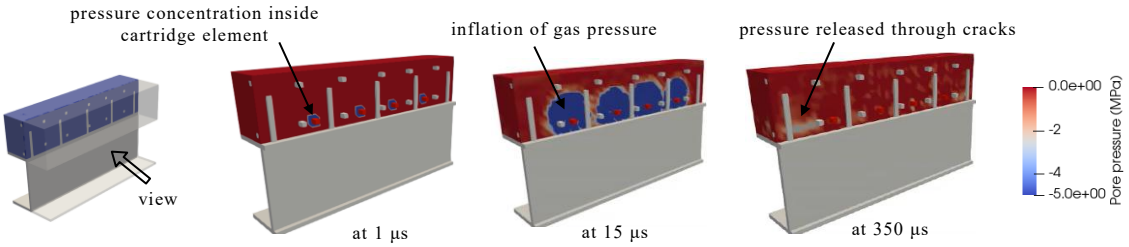
(1) Simulation results for specimen A

The final crack patterns obtained experimentally and numerically immediately after deflagration are compared in **Fig. 3(a)** and **Fig. 3(b)** [10]. Both results exhibit conical cup-shaped fractures extending between the cartridges and the stud dowel heads. The computed principal strain contours closely correspond to the experimentally observed cup-shaped fracture paths, as indicated by the pink lines in **Fig. 3(a)**. In practice, the concrete region situated above the stud dowel heads can be detached and removed as a single block, while the remaining concrete can subsequently be removed with relative ease using manual methods.

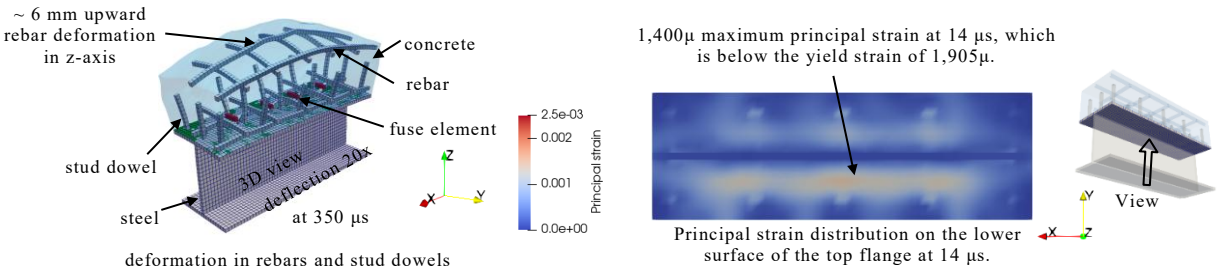


(a) Before and after the action of deflagration in the experiment[9]

(b) Final crack pattern by analysis



(c) Pore pressure inside the specimen in specific time-steps



(d) Deformation in rebars and principal strain in the flange

Fig. 3. Simulation results in a model based on Specimen A

Following self-reactive liquid deflagration, a rapid increase in pore pressure develops in the vicinity of the cartridge (**Fig. 3(c)**)[10], where gas expansion is initially constrained within the surrounding concrete. As cracking progresses, gas begins to flow through the newly formed fracture surfaces. The resulting pressure gradient drives gas migration outward, generating three-dimensional tensile stresses that may contribute to further crack extension. As the gas infiltrates both the pore network and fracture system, pressure accumulates at crack tips, facilitating crack propagation.

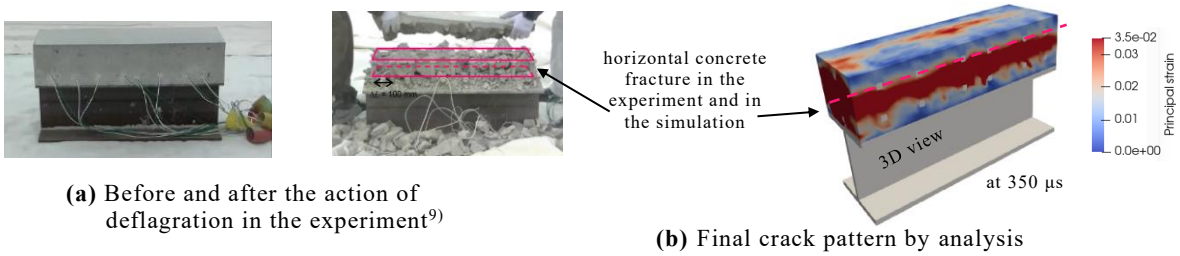
Once cracks reach the free surface, the gas is released to the atmosphere, which is represented as ambient pressure in the numerical simulations.

Gas transport occurs primarily through micro-pores and crack networks because solid inclusions, such as reinforcing bars and stud dowels, are impermeable to gas flow[10]. Consequently, the accumulation of gas pressure can induce deformation in the reinforcing steel and displacement of the surrounding concrete, thereby accelerating crack growth and local concrete crushing, as illustrated in **Fig. 3(d)**. A maximum vertical displacement of approximately 6 mm was observed in the central top reinforcing bar in the z-direction, as shown in the graph presented in **Fig. 3(d)**.

To evaluate the feasibility of reusing the steel girder after demolition, the principal strain obtained from the numerical analysis was examined. As shown in **Fig. 3(d)**, the maximum principal strain reached 1,400μ at 14 μs on the lower surface of the top flange. This value is lower than the yield strain of 1,905μ, indicating that the principal strain remained below the yielding limit and that no yielding occurred. This observation is consistent with the experimental findings reported by[9], suggesting that the steel girder remains suitable for reuse after the deflagration operation.

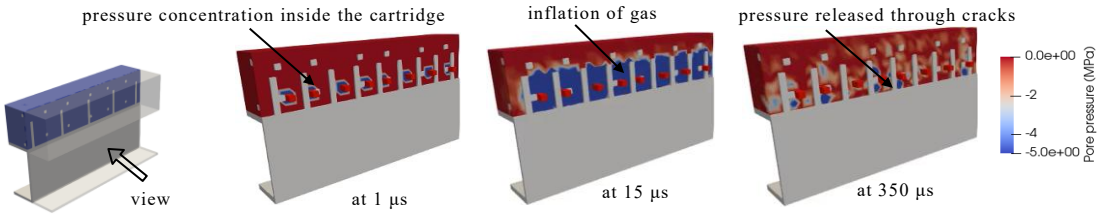
(2) Simulation results for specimen B

Fig. 4(a) and **Fig. 4(b)** compare the final crack configurations obtained from the experimental observations and numerical simulations following deflagration[10]. Extensive concrete crushing developed beneath the stud dowel heads as a result of the high confinement produced by the closely spaced dowels, which restricted gas expansion and caused a rapid increase in internal pressure. This confinement likely created a horizontal restraint zone around the stud dowel heads (**Fig. 4(b)**, pink lines), resulting in the formation of a horizontal fracture plane. Comparable fracture characteristics were also observed in the experimental results shown in **Fig. 4(a)** (pink lines) as reported by 9).

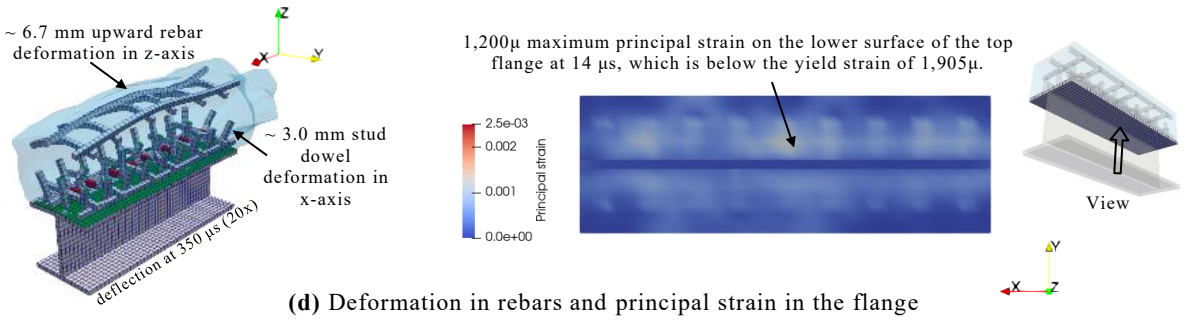


(a) Before and after the action of deflagration in the experiment[9]

(b) Final crack pattern by analysis



(c) Pore pressure inside the specimen in specific time-steps



(d) Deformation in rebars and principal strain in the flange

Fig. 4. Simulation results in a model based on Specimen B

Fig. 4(c) illustrates the generation of pressurized gas, its subsequent expansion, and eventual discharge through the developed fracture network[10]. The numerical results demonstrate a coupled mechanism between gas-pressure-driven crack growth and the reduction in pressure associated with gas escape through the formed cracks. The majority of the pressure relief occurred through the side surfaces of the specimen, owing to the extensive concrete damage in these regions, whereas the upper surface remained comparatively less damaged.

The deformation behavior of the stud dowels and reinforcing bars is presented in **Fig. 4(d)**[10]. The stud dowel located near the edge of the specimen experienced a maximum displacement of approximately 5.2 mm in the x-direction. Following the release of the pressurized gas, this displacement decreased to about 3 mm. Furthermore, the upper reinforcing bar situated at the center of the specimen exhibited a maximum displacement of approximately 6.7 mm in the z-direction, as illustrated in the graph in **Fig. 4(d)**. These deformations in both the stud dowels and reinforcement contributed to the progression of concrete crushing and crack propagation.

As shown in **Fig. 4(d)**, the highest principal strain occurred at the lower surface of the top flange and reached 1,200 μ at 14 μs. Since this value did not exceed the yield strain of 1,905 μ, the steel girder remained within the elastic range throughout the deflagration reaction. This outcome agrees with the experimental observations reported in previous research[9] and demonstrates the potential for steel girder reuse after demolition.

(3) The effect of explosion speed

The coupling of structural concrete with the kinetics of compressible pore media is a relatively recent modeling approach, and its response to variations in explosion characteristics has not yet been fully established. Therefore, in this study, a sensitivity analysis was conducted by varying the explosion speed to evaluate the robustness of the coupled model, examine its response to changes in gas pressurization behavior, and provide a base for future model validation and development.

Detonation (~10^{-5} s), represented by explosives such as TNT, produces intense shock waves that cause severe crushing and fragmentation. Deflagration (~10^{-4} s), such as self-reactive liquid, promotes gas-driven crack propagation and controlled concrete fracture, making it suitable as the reference case in this study. Ballistic loading (~10^{-2} s), generated by projectile or propellant-driven impacts, applies the load over a longer duration, resulting in lower stress-wave intensity, slower crack propagation, and more localized damage.

In this section, the influence of explosion speed on fracture behavior and crack propagation is investigated for Specimen A by modifying the time history of the generated peak pressure, as shown in **Fig. 5**. In the reference model, the pressure peak occurs at 55 μs. In the modified model, the time to reach the peak pressure was increased to 100 times that of the reference case (5,500 μs).

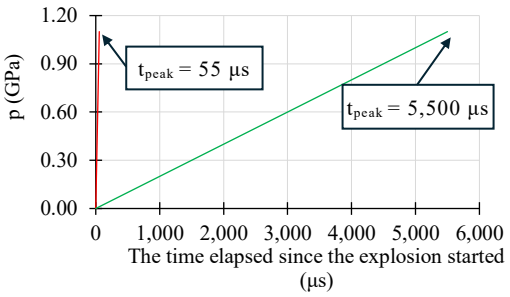
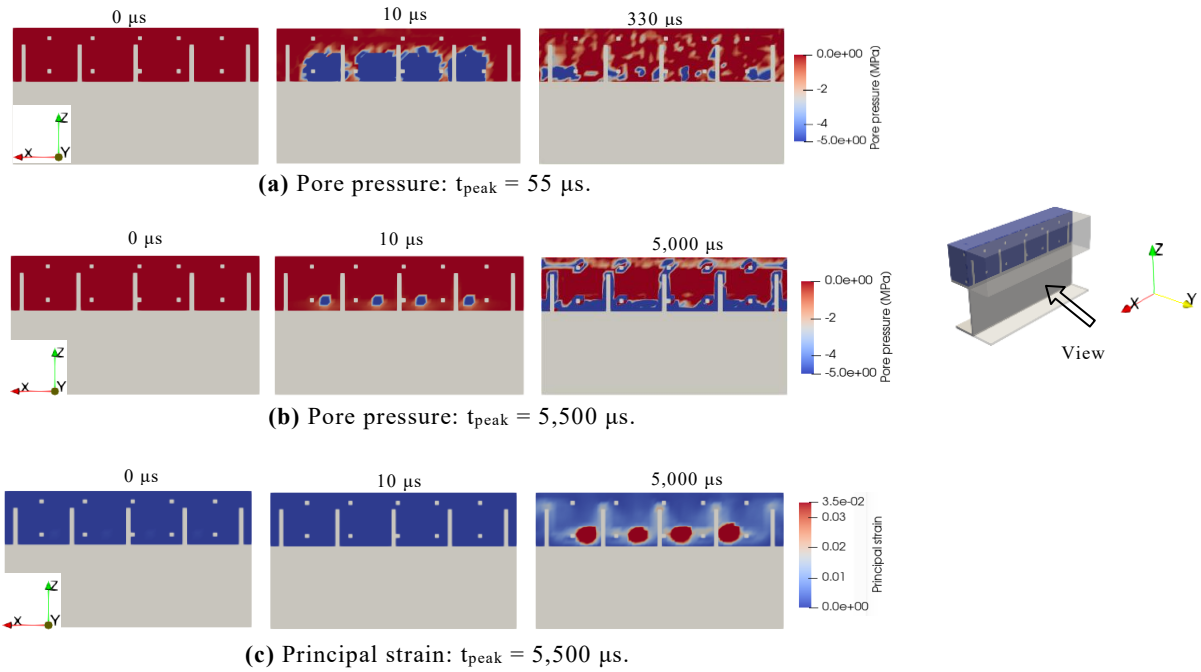


Fig. 5. Adjusted time dependence of peak pressure used in sensitivity analysis

In the modified peak pressure time history, both the pressure rise and subsequent decay are more gradual than those in the reference case, as shown in **Fig. 6(a)** and **Fig. 6(b)**. This smoother pore pressure evolution reduces the intensity of the dynamic loading, thereby suppressing crack initiation and propagation, as illustrated in **Fig. 6(c)**. The slower pressurization rate allows greater energy dissipation within the surrounding material, while the reduced pressure release rate decreases the severity of crack development.

When the pressure peak occurred at 55 μs, the rapid explosion generated high strain rates, leading to an inertia dominated response characterized by severe cracking (**Fig. 3(b)**). In contrast, when the pressure peak was at 5,500 μs, the slower explosion produced lower strain rates, allowing stress redistribution between concrete and steel, reducing dynamic amplification, and causing damage to evolve over a longer duration as shown in **Fig. 6(c)**.



(a) Pore pressure: t_{peak} = 55 μs.

(b) Pore pressure: t_{peak} = 5,500 μs.

(c) Principal strain: t_{peak} = 5,500 μs.

Fig. 6. Pore pressure and principal strain profiles in different time-steps for Specimen A.

5. Conclusion

The numerical simulations reproduced the experimentally observed fracture behavior, demonstrating the capability of the proposed poro-mechanical model to capture the coupled mechanisms of gas-pressure evolution, crack propagation, and concrete failure. The results indicate that closely spaced stud dowels generate strong confinement, leading to elevated pore pressures, localized concrete crushing, and enhanced crack development, while the deformation of reinforcing bars and stud dowels further contributes to fracture progression. Moreover, the interaction between gas-pressure-driven cracking and subsequent pressure release through fracture pathways plays a significant role in the demolition process. Parametric analyses revealed that higher explosion rates produce greater strain rates and inertia effects, resulting in more severe cracking, whereas slower pressure rises promote energy dissipation and stress redistribution, leading to reduced damage intensity. Despite the extensive concrete fracture, the strains in the steel girder remained below the yield limit, confirming their potential for reuse in future renovation applications.

Acknowledgement: The authors would like to express their sincere gratitude to Prof. Koichi Maekawa, Prof. Akira Hosoda and Dr. Akio Kasuga for their valuable guidance and supervision throughout the simulation study.

References

1) Uenishi, K., Wada, K., Yamachi, H., Nakamori, J.: Precisely Controlled Dynamic Disintegration of Steel-Concrete Composite Structures, 5th International Conference on Structural Integrity and Durability, Procedia Structural Integrity, Vol.46, pp.136-142, 2023
2) Sasaki, K., Sakamoto, R., Tanaka, M., Hidani, K., Iizuka, S.: Development of an Electric Discharge Impulse Crushing System, 6th EFEE World Conference on Explosives and Blasting, Vol.6, pp.379-400, Lisbon, Portugal, 2011
3) Tanaka, S., Bataev, I., Inao, D., Hokamoto, K.: Initiation of Nitromethane Deflagration Promoted by the Oxidation Reaction of Vaporized Metal Wire, Applications in Energy and Combustion Science, Vol.1-4, 2020
4) Zažirej, S., Maekawa, K., Hosoda, A.: Poromechanical Approach to Blast-Induced Dynamic Fracture in Concrete,

Structural Concrete, 1-21, 2024

5) Biot, M.A.: General Theory of Three-Dimensional Consolidation. Journal of Applied Physics, Vol.12, pp.155-164, 1941
6) Biot, M.A.: Theory of Stability and Consolidation of a Porous Medium Under Initial Stress, Journal of Mathematics and Mechanics, Vol.12, pp.521-541, 1963
7) Maekawa, K., Ishida, T., Kishi, T.: Multi-scale Modeling of Structural Concrete, Oxford: Taylor & Francis, 2008
8) Yamanoi, Y., Maekawa, K.: Disintegration of Low and Normal Strength Concrete in Shear Localized Bands and Its Constitutive Modeling, Engineering Structures, Vol.266, 2022
9) Wada, K., Uenishi, K., Yamachi, H., Nakamori, J.: On Wave-Controlled Dynamic Disintegration of Steel-Concrete Composite Structures, Proceedings of the 15th National Symposium on Rock Mechanics, Vol.89, pp.505-508, 2021
10) Addisu, B., Hosoda, A., Maekawa, K., Stanislav, Z.: A Numerical Analysis of Blast-Induced Dynamic Fracture in Steel-Concrete Composite Structures, 8th International Conference on Structural Integrity and Durability (ICSID2025), Vol.82, pp.30-36, 2026
11) Maekawa, K., Pimanmas, A., Okamura, H.: Nonlinear Mechanics of Reinforced Concrete. Oxford: Taylor & Francis, pp.30-31, 2003